Sanfilippo syndrome type B, a lysosomal storage disease, is also a tauopathy

Kazuhiro Ohmi[a], Lili C. Kudo[b], Sergey Ryazantsev[a,c], Hui-Zhi Zhao[a], Stanislav L. Karsten[b,d,e,1,2], and Elizabeth F. Neufeld[a,1,2]

Departments of [a]Biological Chemistry, [b]Neurology and [e]Obstetrics and Gynecology, David Geffen School of Medicine at University of California at Los Angeles, Los Angeles, CA 90095; [c]Electron Imaging Center for Nanomachines at California NanoSystems Institute, University of California at Los Angeles, Los Angeles, CA 90095; [d]Division of Neuroscience, Los Angeles Biomedical Research Institute at Harbor-University of California at Los Angeles Medical Center, Torrance, CA 90502

Contributed by Elizabeth F. Neufeld, March 24, 2009 (sent for review February 15, 2009)

Sanfilippo syndrome type B (mucopolysaccharidosis III B, MPS III B) is an autosomal recessive, neurodegenerative disease of children, characterized by profound mental retardation and dementia. The primary cause is mutation in the *NAGLU* gene, resulting in deficiency of α-*N*-acetylglucosaminidase and lysosomal accumulation of heparan sulfate. In the mouse model of MPS III B, neurons and microglia display the characteristic vacuolation of lysosomal storage of undegraded substrate, but neurons in the medial entorhinal cortex (MEC) display accumulation of several additional substances. We used whole genome microarray analysis to examine differential gene expression in MEC neurons isolated by laser capture microdissection from *Naglu*$^{-/-}$ and *Naglu*$^{+/-}$ mice. Neurons from the lateral entorhinal cortex (LEC) were used as tissue controls. The highest increase in gene expression (6- to 7-fold between mutant and control) in MEC and LEC neurons was that of *Lyzs*, which encodes lysozyme, but accumulation of lysozyme protein was seen in MEC neurons only. Because of a report that lysozyme induced the formation of hyperphosphorylated tau (P-tau) in cultured neurons, we searched for P-tau by immunohistochemistry. P-tau was found in MEC of *Naglu*$^{-/-}$ mice, in the same neurons as lysozyme. In older mutant mice, it was also seen in the dentate gyrus, an area important for memory. Electron microscopy of dentate gyrus neurons showed cytoplasmic inclusions of paired helical filaments, P-tau aggregates characteristic of tauopathies—a group of age-related dementias that include Alzheimer disease. Our findings indicate that the Sanfilippo syndrome type B should also be considered a tauopathy.

hyperphosphorylated tau | lysozyme | mucopolysaccharidosis | entorhinal cortex | gene expression microarray

The Sanfilippo syndrome type B (mucopolysaccharidosis III B, MPS III B) is an autosomal recessive disorder caused by mutations in the NAGLU gene, which encodes the lysosomal enzyme α-*N*-acetylglucosaminidase (reviewed in ref. 1). The resulting deficiency of the enzyme causes lysosomal accumulation of its substrate, heparan sulfate. The disease is genetically heterogeneous, with over a hundred mutations recorded to date (The Human Gene Mutation Database at the Institute of Medical Genetics in Cardiff http://www.hgmd.cf.ac.uk/ac/index.php). Affected children have profound mental retardation, intractable behavior problems, and eventual dementia, although somatic manifestations are relatively mild; death usually occurs in the second decade (2). The clinical manifestations of MPS III B are similar to those of MPS III A, MPS III C, and MPS III D, which are the result of other enzymatic deficiencies in the lysosomal degradation of heparan sulfate. There is no effective therapy for any form of MPS III.

A mouse model of MPS III B had been created by homologous recombination for the purpose of studying the pathophysiology of the disease and for developing treatment (3). The mutant (*Naglu*$^{-/-}$) mice are healthy when young but have limited fertility and a shortened lifespan (about 8 months). They manifest some behavioral anomalies, which have been variously reported as hypoactivity (3) and hyperactivity (4); the difference is probably because of different ages of the animals studied and different methods of testing. Other data show altered circadian rhythm, hearing and vision deficits and, in older mice, a loss of Purkinje cells and impaired motor coordination (5).

Gene therapy has been tested in the mice with some success (4, 6–8) but is unlikely to be available for human patients in the near future. The disease is recessive and heterozygous mice have a normal phenotype.

Pathological abnormalities in the brain of *Naglu*$^{-/-}$ mice have been a major focus of research because they have the greatest potential for explaining the neurodegeneration in human patients. Astrocytes and microglia are activated (9–11), as is the entire immune system in the brain (12). Accumulation of the primary storage product, heparan sulfate, is low (9), but can be detected histochemically by colloidal iron staining (13). Some *Naglu*$^{-/-}$ neurons also accumulate GM3 ganglioside and cholesterol (10, 14), ubiquitin, and a lysosomal form of subunit c of mitochondrial ATP synthase (SCMAS) (13). The accumulation of these secondary products and of the primary product is not dispersed throughout the brain, but is limited to neurons in certain areas, especially layer II of the medial entorhinal cortex and to a lesser extent, layer V of the somatosensory cortex. There is no obvious explanation for the accumulation of these apparently unrelated substances and for the focal nature of the accumulation.

On the hypothesis that something in the cellular environment of neurons in the medial entorhinal cortex (MEC) of *Naglu*$^{-/-}$ mice made them prone to accumulate these materials, we undertook to examine gene expression in those cells and to follow up candidate findings by examining protein expression. We used laser capture microdissection to obtain neuronal cell bodies, microarray-based technology to detect changes in gene expression, and immunohistochemistry to examine proteins. Neurons of the lateral entorhinal cortex (LEC) of *Naglu*$^{-/-}$ mice, which do not contain the secondary accumulations, were used as controls for area-specific differences, while neurons of both MEC and LEC of heterozygous mice were used as controls for differences because of the disease. This approach yielded some

Author contributions: K.O., S.L.K., and E.F.N. designed research; K.O., L.C.K., S.R., H.-Z.Z., and S.L.K. performed research; K.O., L.C.K., S.R., S.L.K., and E.F.N. analyzed data; and K.O., L.C.K., S.L.K., and E.F.N. wrote the paper.

The authors declare no conflict of interest.

Freely available online through the PNAS open access option.

Data deposition: The microarray data have been deposited in the Gene Expression Omnibus database http://www.ncbi.nlm.nih.gov/geo/ (accession no GSE15758).

[1]S.L.K. and E.F.N. contributed equally to this work.

[2]To whom correspondence may be addressed. E-mail: eneufeld@mednet.ucla.edu or skarsten@ucla.edu.

This article contains supporting information online at www.pnas.org/cgi/content/full/0903223106/DCSupplemental.

Table 1. Differential gene expression in neurons of the MEC and LEC regions of the brain of Naglu$^{-/-}$ mice

Accession	Gene symbol	MEC	*p* value	LEC	*p* value
NM_017372	Lyzs	6.93	0.0002	6.16	0.002
NM_021281	Ctss	2.2	0.00	2.3	0.02
NM_147217	Gprc5c	2.5	0.05	2.0	-
AK083103	Mobp	2.2	0.04	1.2	-
NM_031254	Trem2	2.0	0.02	1.6	-
NM_025745	4933407N01Rik	1.9	0.02	1.3	-
NM_026380	Rgs8	1.9	0.00	1.4	-
NM_022980	Dscr1l2	1.8	0.03	2.0	-
NM_031998	Tsga14	1.8	0.05	1.1	-
AK047894	Cit	1.8	0.02	1.2	-
NM_010700	Ldlr	1.8	0.03	1.3	-
NM_007694	Chgb ($n = 5$)	1.8	<0.01	1.5	-
AK038529	Cdh4	3.8	-	2.8	0.04
NM_001037727	Arhgap25	1.3	-	2.7	0.04
XM_885736	Fat1	3.8	-	2.6	0.01
NM_080728	Myh7 ($n = 2$)	1.0	-	2.3	<0.05
AK017596	EST, unknown	2.1	-	1.9	0.03
NM_008528	Blnk	1.6	-	1.9	0.00
NM_027518	Gpr137c	−1.1	-	1.9	0.00
NM_172443	Tbc1d16	1.3	-	1.9	0.04
NT_039170	Gls	1.3	-	1.9	0.04
NM_010271	Gpd1	1.3	-	1.9	0.02
NM_008380	Inhba	1.3	-	1.8	0.04
AK150790	H2-K1	1.5	-	1.8	0.00
AK020521	Gorasp2	1.0	-	1.8	0.04
AK078617	Trps1	1.0	-	−1.8	0.02
NM_001045520	Clint1	1.1	-	−1.8	0.01

Results are expressed as an average fold change of *Naglu*$^{-/-}$ vs. *Naglu*$^{+/-}$ in 3 independent experiments (3 different pairs of animals) for MEC and LEC. Significance was calculated using paired *t* test ($P < 0.05$). The *p* value is not shown when significance was not reached ($P > 0.05$). The number of unique microarray probes for a given gene (*n*) is specified if greater than 1

unexpected findings of increased lysozyme and P-tau in the MEC and P-tau with paired helical filaments in the dentate gyrus of the mutant mice, which may require reassessment of the pathogenesis of the disease.

Results

Elevated Expression of the Gene Encoding Lysozyme Is Found in Neurons of the Medial Entorhinal Cortex and Lateral Entorhinal Cortex. To identify factors in the cellular environment that might contribute to secondary accumulations in neurons of the MEC of *Naglu*$^{-/-}$ mice, transcripts from these neurons were compared by microarray technology with those of MEC neurons from unaffected (heterozygous) mice. Neurons were collected by laser capture microdissection from 2-month-old female mice, 3 from each group. In addition, transcripts from neurons in LEC, a neighboring area in which there are no secondary accumulations, were also examined. We identified 2 genes of which the transcripts were enriched in both MEC and LEC, 10 enriched in MEC only, and 15 enriched in LEC only (Table 1). Two transcripts in MEC (Gprc5c and Dscr112) and 3 transcripts in LEC (Cdh4, Fat1, and EST AK017596) showed a trend toward overexpression in *Naglu*$^{-/-}$ but did not reach statistical significance. Table 1 shows that the highest expression was found for *Lyzs*, the gene encoding lysozyme (6.93, $P = 0.0002$ and 6.16, $P = 0.002$ for the MEC and LEC, respectively). Other transcripts were elevated 2.8-fold or less.

Lysozyme Protein Is Seen in Neurons of the Medial, but Not the Lateral Entorhinal Cortex. The presence of lysozyme protein in MEC neurons of a *Naglu*$^{-/-}$ mouse was verified by double staining, using NeuroTrace as neuronal marker (green) and antibody against mouse lysozyme (red) (Fig. 1 *A–C*). Immunohistochemistry also showed that even though lysozyme transcripts were almost equally elevated in the MEC and LEC neurons of the mutant mouse, the lysozyme protein was seen in the mutant mouse MEC (Fig. 1*D*) but not in LEC (Fig. 1*E*). As expected, it was not present in neurons of the control mouse MEC (Fig. 1*F*) or LEC (data not shown). While Fig. 1*D* shows staining in MEC neurons of a mouse that was 6 months old, lysozyme was already present in MEC neurons of a 1-month-old *Naglu*$^{-/-}$ mouse, although the staining was not as intense (data not shown). As expected from earlier studies (10), lysozyme was also prominent in microglia (identified by antibody to CD68) of the mutant mouse, in MEC (Fig. S1), in LEC, and in many other areas of the brain (data not shown).

Hyperphosphorylated Tau Is Found in Neurons of the Medial, but Not Lateral Entorhinal Cortex. Exposure of cultured rat neurons to oligomers of hen egg white lysozyme had been shown to induce the hyperphosphorylation of tau in cultured rat neurons, as determined by reactivity with antibodies raised against hyperphosphorylated tau epitopes in Alzheimer disease (15). On the hypothesis that accumulation of endogenous lysozyme might act in a similar way, we tested for the presence of hyperphosphorylated tau, using commercially available antibodies against human hyperphosphorylated tau. Indeed, hyperphosphorylated tau was detected with anti-P-tau AT100 in MEC neurons (layer II) of the mutant mouse brain (Fig. 1*G*), but neither in LEC neurons of the same brain (Fig. 1*H*) nor in MEC neurons of the control mouse brain (Fig. 1*I*). The presence of P-tau thus followed the presence of lysozyme protein, and the two proteins were found in the same cells by double immunostaining (Fig. 1 *J–L*). P-tau was also found in the same cells as SCMAS (Fig. 1 *M–O*), one of the proteins accumulated secondarily in MEC

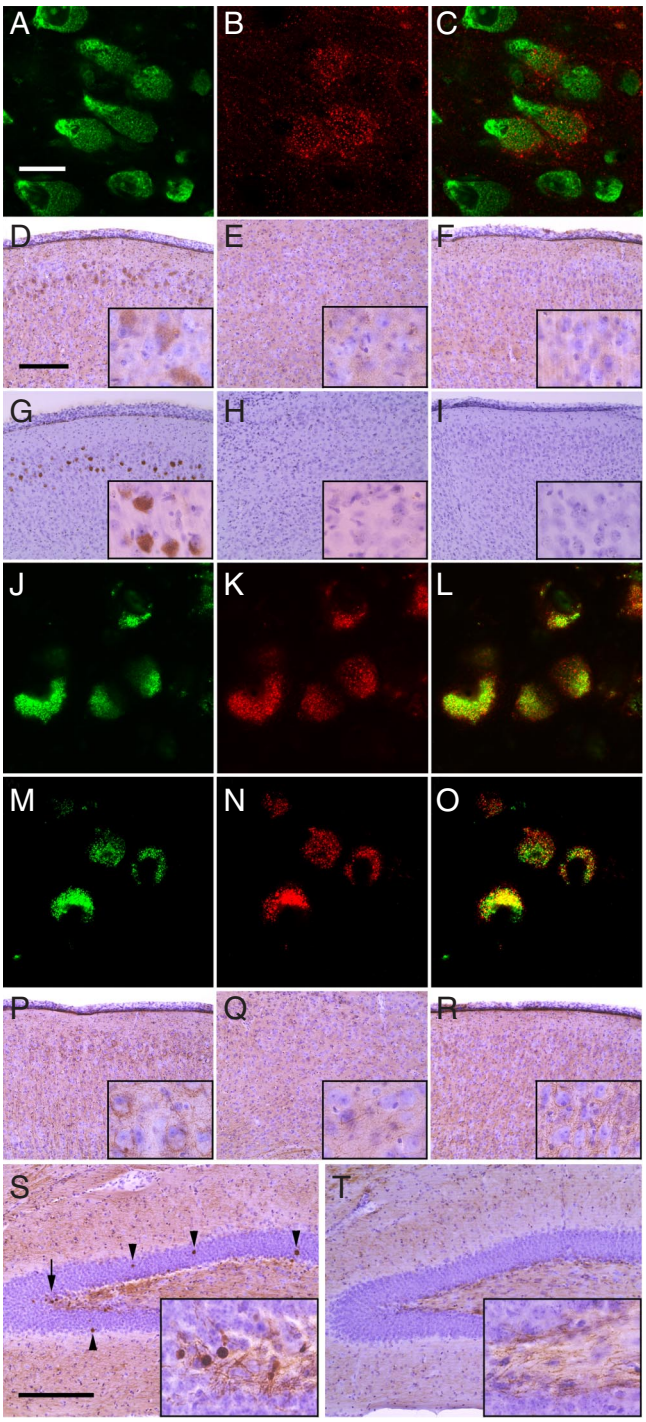

Fig. 1. Lysozyme and P-tau in *Naglu*$^{-/-}$ and control mouse brain. (*A–C*) Confocal images of cells in MEC of *Naglu*$^{-/-}$ mouse brain stained with (*A*) NeuroTrace, a marker for neurons, (*B*) with antibody against lysozyme, (*C*) merged images of *A* and *B*. (Scale bar, 20 μm.) (*D–F*) Immunohistochemistry with lysozyme antibody of (*D*) *Naglu*$^{-/-}$ MEC, (*E*) *Naglu*$^{-/-}$ LEC, and (*F*) *Naglu*$^{+/-}$ MEC. (Scale bar, 200 μm.). *Insets* are at 4 times higher magnification. (*G–I*) Immunohistochemistry with P-tau antibody AT100 of (*G*) *Naglu*$^{-/-}$ MEC, (H) *Naglu*$^{-/-}$ LEC, and (I) *Naglu*$^{+/-}$ MEC. (Scale as in *D*.) (*J–L*) Confocal images of neurons in *Naglu*$^{-/-}$ MEC immunostained with (*J*) P-tau antibody AT100, (*K*) lysozyme antibody, and (*L*) merged image of *J* and *K*. (Scale as in *A*.) (*M–O*) Confocal images of *Naglu*$^{-/-}$ neurons immunostained with (*M*) P-tau antibody AT100, (*N*) SCMAS antibody, and (*O*) merged image of *M* and *N*. (Scale as in *A*.) (*P–R*) Immunohistochemistry with P-tau antibody AT270 of (*P*) *Naglu*$^{-/-}$ MEC, (*Q*) *Naglu*$^{-/-}$ LEC, and (*R*) *Naglu*$^{+/-}$ MEC. (Scale as in *D*.) (*S–T*) Immunohistochemistry with P-tau antibody AT270 of dentate gyrus of (*S*) *Naglu*$^{-/-}$ mouse and (*T*) *Naglu*$^{+/-}$ mouse; arrowheads indicate round bodies, while the arrow indicates area shown in inset. (Scale bar, 200 μm.)

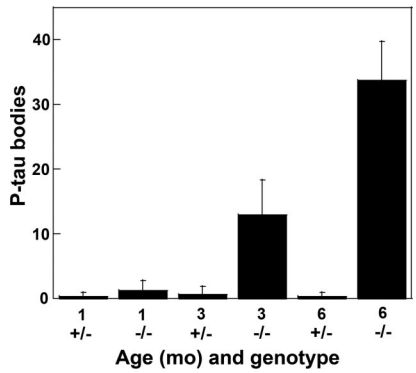

Fig. 2. Age-dependent increase in P-tau positive bodies in the dentate gyrus of mutant brain. The graph shows the number of round bodies detected with antibody AT270 in the dentate gyrus of *Naglu*$^{-/-}$ and *Naglu*$^{+/-}$ mice at 1, 3, and 6 months. A total of 6 fields from each mouse were used for counting after immunostaining as shown in Fig. 1 *S* and *T*. The bars show the mean ± SD for 3 mice.

neurons (13). While AT100 stained the soma, a second antibody, AT270, reacted mainly (although not exclusively) with dendrites of MEC neurons (Fig. 1 *P–Q*). Some background staining in control neurons was seen with AT270, which cross-reacts weakly with normal tau, in contrast to AT100, which has no such cross-reactivity (16). Several other P-tau antibodies tested—AT8 and AT180, and AnaSpec 54960 and -54961 (see *Materials and Methods*)—did not stain the *Naglu*$^{-/-}$ MEC neurons, showing that not all of the Alzheimer hyperphosphorylation sites are used.

Hyperphosphorylated Tau Is Found in the Dentate Gyrus. Numerous round bodies staining prominently for P-tau with AT270 could be seen in the dentate gyrus (DG) of 6 month-old mice (Fig. 1*S*), whereas these bodies were seen only rarely in the DG of the control mice (Fig. 1*T*). The size of the P-tau positive bodies is roughly similar to that of the granular neurons among which they are found. Their accumulation in the DG is age dependent, as shown in Fig. 2.

Examination by electron microscopy of ultrathin sections derived from the DG of *Naglu*$^{-/-}$ mice revealed the presence of intracellular filamentous inclusions that have the characteristics of paired helical filaments (PHF) (Fig. 3). The diameter of the filaments was ≈14–15 nm. The paired filament inclusions were found in neuronal cell bodies (Fig. 3) and also in dendrites and axons (data not shown). In the cell bodies, they were in the cytosol and not associated with any specific organelle. Astrocytes, microglia, and endothelial cells did not contain such inclusions (data not shown).

Discussion

Abnormal accumulations found in neurons of the MEC and of the dentate gyrus of the MPS III B mouse model are summarized in Fig. 4. To the MEC accumulation of 5 metabolites (GAG, cholesterol, GM3 ganglioside, ubiquitin, and SCMAS) described previously (13), we have added an accumulation of lysozyme and P-tau. Other than GAG detected by colloidal iron and presumed to be heparan sulfate, the primary storage product because of lack of α-*N*-acetylglucosaminidase activity, all accumulations are secondary. These accumulations occur in the same cells (although not necessarily in the same organelles) as shown by the colocalization of AT100 staining with lysozyme and with SCMAS (Fig. 1) and the earlier finding of colocalization of SCMAS with GM3 ganglioside and ubiquitin (13). But the temporal relationship of these accumulations has not been determined. The induction of P-tau follows exposure to exogenous lysozyme

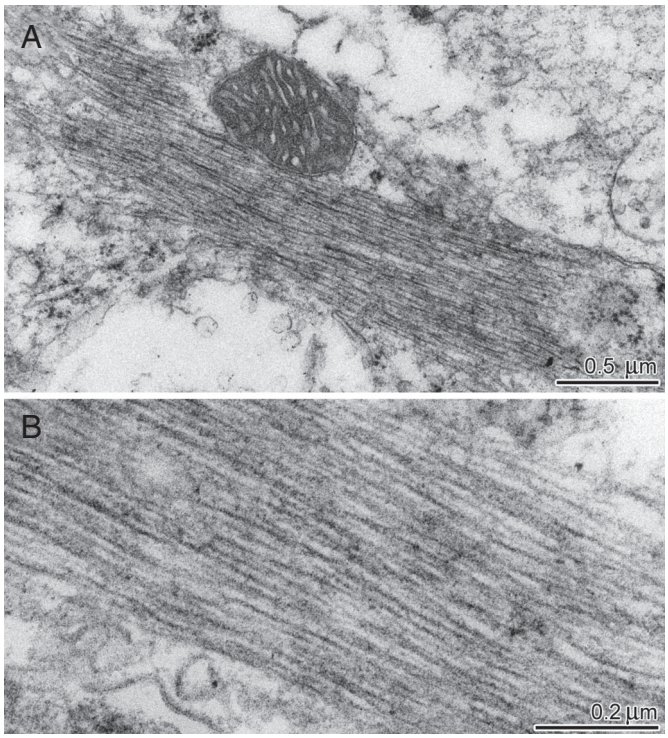

Fig. 3. Inclusion in neuron of dentate gyrus of a *Naglu*$^{-/-}$ mouse, viewed by electron microscopy. (*A*) Proximity to the mitochondrion in *A* confirms that the inclusion is intracellular; the higher magnification of *B* shows the resemblance to paired helical filaments.

(15), and this may also be the case for endogenous lysozyme. We do not know whether induction of lysozyme itself occurs before, after, or concurrently with the accumulation of GM3 ganglioside, cholesterol, ubiquitin, and SCMAS.

Lysozyme, an enzyme needed to break down the peptidoglycan of bacterial cell walls, is present in phagocytes (neutrophils and macrophages) and in secretions of epithelial cells (tears and saliva), where it serves as a host defense against bacterial infection (17, 18). Microglia, cells of macrophage lineage that reside in brain, overexpress lysozyme mRNA when activated, as part of the inflammation that accompanies lysosomal storage disease (10, 12). Lysozyme was not previously shown to be present in neurons and the reason for the marked elevation of *Lyzs* expression in *Naglu*$^{-/-}$ neurons is not known. Perhaps the inflammatory process initiated by lysosomal engorgement also induces synthesis of inflammation-related genes and proteins by neurons.

Although the *Lyzs* transcript was similarly elevated in MEC and LEC neurons, accumulation of the protein was observed only in MEC. The simplest explanation is that turnover of the protein is impeded in MEC neurons, perhaps because of the presence of the other accumulated metabolites. Lysozyme is known to be amyloidogenic, i.e., prone to form aggregates that have the property of amyloid and are resistant to degradation (for review see ref. 19). A small decrease in the turnover rate in MEC may allow lysozyme to reach a critical concentration to form such aggregates, thus further reducing its degradation and promoting an increase in the amount of lysozyme stored in the cytoplasm. Another possible explanation is that the small difference in the amount of lysozyme mRNA between MEC and LEC may translate to a slightly higher rate of lysozyme synthesis in MEC, allowing the lysozyme to reach the critical concentration required for aggregation. The two explanations are not mutually exclusive.

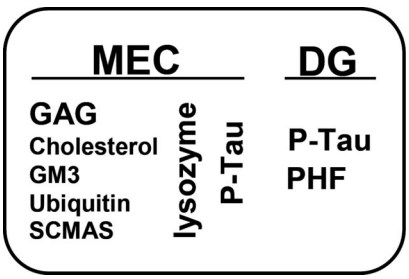

Fig. 4. Schematic summary of abnormalities detected in the brain of the *Naglu*$^{-/-}$ mouse.

How lysozyme induces the hyperphosphorylation of tau is another aspect that is not understood. Are there signals that emanate from lysozyme accumulation, or do lysozyme aggregates serve as a template for the aggregation of tau and its phosphorylation? It has been suggested that it is lysozyme in the form of oligomers rather than lysozyme amyloid that is the tau hyperphosphorylation-inducing factor (15). But that could be a matter of entry of the exogenous lysozyme into cells, an issue that might not apply to the accumulation of endogenous enzyme.

Another unanswered question is the origin of hyperphosphorylated tau in the DG. That area of the brain was not enriched in lysozyme in mice of any age examined—1, 3, and 6 months (data not shown), suggesting that it might have received an inductive signal from the MEC or that the hyperphosphorylated tau actually migrated from the MEC to the DG. The migration hypothesis is supported by our finding of PHF in axons and by the known communication between MEC and the DG (reviewed in refs. 20, 21). Because the DG is important in the storage of memory, interference with its function is considered an important cause of dementia (for review, see refs. 22–25).

Others have looked for but did not find hyperphosphorylated tau in brain of human MPS patients or animal models (26, 27). From our experience with the MPS III B mouse model, we believe that hyperphosphorylated tau can be easily missed. It is found in a very small area of the brain, it reacts only with some of the antibodies prepared against hyperphosphorylated tau in Alzheimer disease, and even with these antibodies, immunoreactivity is affected by the preparation of the sections. For example, AT100 did not stain MEC neurons when the brains had been embedded in paraffin and had to be used with vibratome sections, whereas AT270 could be used with both paraffin and vibratome sections. Therefore the possible presence of hyperphosphorylated tau in brain of patients affected by MPS III B and other lysosomal storage diseases, and of animal models of these diseases, should be reexamined.

Our unexpected findings were made possible by our choice of cell-specific microarray analysis to ask why neurons in MEC accumulated several apparently unrelated metabolites and proteins. Although we have not yet obtained an answer to that question, we discovered neuronal accumulation of yet another protein, lysozyme in MEC; this led to the further finding of hyperphosphorylated tau in neurons of MEC and of the dentate gyrus. It was the unbiased nature of the microarray results, combined with the use of a selected neuronal population, which made us consider, against prevailing dogma, that lysozyme in brain was not a product solely of microglia but was also made by neurons.

Hyperphosphorylated tau and PHF (aggregates of hyperphosphorylated tau) are present in many diseases associated with dementia. This group of diseases, named "tauopathies," includes Niemann-Pick disease type C, the only lysosomal storage disease in which hyperphosphorylated tau has been reported to date (28). There are 9 other tauopathies, including Alzheimer disease

(reviewed in ref. 29). In view of the public health implications of the high and increasing incidence of Alzheimer disease, we expect to see the development of drugs to prevent the formation of paired helical filament or perhaps even to dissolve them after they have formed. A rare disorder such as MPS III B can only benefit from the anticipated wealth of research for therapy of Alzheimer disease.

Materials and Methods

Mice and Tissue Collection. A mouse colony of MPS III B, created by targeted disruption of the *Naglu* gene and placed on a C57BL/6 background, was the source of mutant (*Naglu*$^{-/-}$) and control (*Naglu*$^{+/-}$) mice (3). The animal studies were approved by the Chancellor's Animal Research Committee. For isolation of neurons by laser capture microdissection (LCM) and subsequent RNA analysis, mice were killed with excess pentobarbital, decapitated, and the brain removed as rapidly as possible. Hemispheres were briefly frozen in 2-methylbutane at −10 °C and stored at −80 °C until use. They were then cut sagittally on a cryostat to 12 μm thickness onto noncharged slides. The slides were stored at −80 °C. Immediately before use of the LCM, the slides were put through a series of washes in the following order: 75% ethanol, H_2O, cresyl violet, a series of ethanol dehydration steps followed by xylene. Identification of MEC and LEC on the cresyl violet (Nissl)-stained slides was accomplished with the guidance of an anatomical atlas (30), as shown in Fig. S2. Harvesting of MEC and LEC neurons was performed using optimized parameters for the PixCell IIe LCM System (31).

For collection of tissue for microscopy, mice were deeply anesthetized with pentobarbital and perfused from the left ventricle with PBS. Perfusion was continued with 3.7% phosphate-buffered formalin for subsequent light microscopy and with 4% formaldehyde–0.1% glutaraldehyde for electron microscopy.

RNA Isolation, Amplification, and Labeling. RNA isolation for the LCM cells was performed using Qiagen RNeasy Micro kit with a slight modification of the manufacturer's protocol for optimal yield. Up to 3 cap linings containing 500 cells were removed and placed in 75 μL of RNA Lysis Tissue buffer (RLT, Qiagen) on ice until all cells were collected. Subsequently, 75 μL of RLT containing β-mercaptoethanol were added before proceeding with the Qiagen protocol. Amplification and labeling of the RNA samples were performed using the Agilent Low RNA Input Linear Amplification Kit PLUS, and the quality of the labeled cRNA was checked using the Agilent 2100 Bioanalyzer (31) (Fig. S3). The purified labeled cRNA targets were mixed and simultaneously hybridized to the microarray.

Microarray Hybridization and Data Analysis. Comparisons were made between 3 pairs of mutant and control littermates for MEC and LEC neurons with dye switch duplicates, for a total of 12 microarrays. Images were scanned using the Agilent DNA microarray scanner and processed with the accompanying software with its default settings to generate processed (global lowess normalized) signal values. Two relatively stringent criteria were used for the identification of differentially regulated genes in MEC and LEC neurons of *Naglu*$^{-/-}$ mice (32, 33). Gene expression changes were required to pass a ratio beyond 95% confidence interval derived from multiple homotypic comparisons (n = 12) (34) between independent biological replicates hybridized onto different arrays, which corresponded to a ratio of 1.8-fold differential expression and a paired t test ($P < 0.05$).

Antibodies. Rabbit antiserum against the recombinant mouse lysozyme P and its preimmune serum were gifts from T. Ganz (University of California at Los Angeles); this antiserum cross-reacts with lysozyme M (35). The following mouse monoclonal antibodies against human P-tau, designated by clone number and phosphorylated amino acid contained in the epitope, were obtained from Pierce/Endogen/Thermo Scientific: AT8 (Ser-202/Thr-205), AT100 (Ser-212/Thr-214), AT180 (Thr-231/Ser-235), and AT270 (Thr-181). The following polyclonal antibodies raised against synthetic peptides containing P-Thr-181 were obtained from AnaSpec. A rat monoclonal antibody against mouse CD68 was purchased from AbD Serotec. A polyclonal antibody against SCMAS was previously described (13).

Secondary antibodies conjugated with biotin and BSA were from Jackson ImmunoResearch Laboratories. Secondary antibodies conjugated to Alexa dye, Prolong-Gold antifade reagent and NeuroTrace 500/525 green were from Molecular Probes/Invitrogen. Vecstatin Elite ABC kit, diaminobenzidine (DAB), Vectabond, and hematoxylin were from Vector Laboratories.

Preparation of Samples for Light Microscopy and Confocal Microscopy. Six month-old mice were used unless otherwise specified. After perfusion (see above), brains were postfixed in formalin at 4 °C. Sections, 40 μm thick, were cut sagittally on vibratome VT1000S (Leica Microsystems). For immunohistochemistry, slices were attached to Vectabond-coated glass slides and permeabilized with ice-cold methanol, washed in 0.3% H_2O_2, and reacted with primary antibody and biotin-labeled F(ab′)$_2$ donkey secondary antibody. The signal was detected by the Vecstatin ABC Elite kit, visualized with DAB (brown color in Fig. 1) and counterstained with hematoxylin (blue color for nuclei). For antibody against P-Tau clone AT100, slices were additionally pretreated with 1% Triton X-100. For double staining, slices were permeabilized and incubated sequentially with antibody or NeuroTrace, and a secondary antibody conjugated to Alexa 488 (green color in Fig. 1). Then they were reacted with another antibody and a secondary antibody conjugated to Alexa 647 (red color in Fig. 1). Images were acquired by laser scanning confocal microscopy (Zeiss Pascal Confocal) and processed by AxioVision software (Carl Zeiss Microimaging) and Adobe Photoshop.

Preparation of Sample for Electron Microscopy. The procedure used was the same as that previously described (10).

ACKNOWLEDGMENTS. We thank Dr. Tomas Ganz (University of California at Los Angeles) for antibodies against mouse lysozyme. This work was supported in part by a National Institutes of Health Grant NS022376 (to E.F.N.), a grant from the Children's Medical Research Foundation (to E.F.N.), a National Alliance for Research on Schizophrenia and Depression (NARSAD) Young Investigator Award (to S.L.K.), and an Alzheimer Association New Investigator Research Grant (to S.L.K.).

1. Neufeld EF, Muenzer J (2001) The mucopolysaccharidoses. *The Metabolic and Molecular Bases of Inherited Disease*, eds Scriver CR, Beaudet AL, Sly WS, Valle D (McGraw-Hill, New York), 8th Ed, pp 3421–3452.
2. Cleary MA, Wraith JE (1993) Management of mucopolysaccharidosis type III. *Arch Dis Child* 69:403–406.
3. Li HH, et al. (1999) Mouse model of Sanfilippo syndrome type B produced by targeted disruption of the gene encoding alpha-N-acetylglucosaminidase. *Proc Natl Acad Sci USA* 96:14505–14510.
4. Cressant A, et al. (2004) Improved behavior and neuropathology in the mouse model of Sanfilippo type IIIB disease after adeno-associated virus-mediated gene transfer in the striatum. *J Neurosci* 24:10229–10239.
5. Heldermon CD, et al. (2007) Development of sensory, motor and behavioral deficits in the murine model of Sanfilippo syndrome type B. *PLoS ONE* 2:e772.
6. Zheng Y, et al. (2004) Retrovirally transduced bone marrow has a therapeutic effect on brain in the mouse model of mucopolysaccharidosis IIIB. *Mol Genet Metab* 82:286–295.
7. Di Natale P, et al. (2005) Treatment of the mouse model of mucopolysaccharidosis type IIIB with lentiviral-NAGLU vector. *Biochem J* 388:639–646.
8. Fu H, et al. (2007) Significantly increased lifespan and improved behavioral performances by rAAV gene delivery in adult mucopolysaccharidosis IIIB mice. *Gene Ther* 14:1065–1077.
9. Li HH, Zhao HZ, Neufeld EF, Cai Y, Gomez-Pinilla F (2002) Attenuated plasticity in neurons and astrocytes in the mouse model of Sanfilippo syndrome type B. *J Neurosci Res* 69:30–38.
10. Ohmi K, et al. (2003) Activated microglia in cortex of mouse models of mucopolysaccharidoses I and IIIB. *Proc Natl Acad Sci USA* 100:1902–1907.
11. Villani GR, et al. (2007) Cytokines, neurotrophins, and oxidative stress in brain disease from mucopolysaccharidosis IIIB. *J Neurosci Res* 85:612–622.
12. DiRosario J, et al. (2009) Innate and adaptive immune activation in the brain of MPS IIIB mouse model. *J Neurosci Res* 87:978–990.
13. Ryazantsev S, Yu WH, Zhao HZ, Neufeld EF, Ohmi K (2007) Lysosomal accumulation of SCMAS (subunit c of mitochondrial ATP synthase) in neurons of the mouse model of mucopolysaccharidosis III B. *Mol Genet Metab* 90:393–401.
14. McGlynn R, Dobrenis K, Walkley SU (2004) Differential subcellular localization of cholesterol, gangliosides, and glycosaminoglycans in murine models of mucopolysaccharide storage disorders. *J Comp Neurol* 480:415–426.
15. Vieira MN, et al. (2007) Soluble oligomers from a non-disease related protein mimic Abeta-induced tau hyperphosphorylation and neurodegeneration. *J Neurochem* 103:736–748.
16. Zheng-Fischhofer Q, et al. (1998) Sequential phosphorylation of Tau by glycogen synthase kinase-3beta and protein kinase A at Thr212 and Ser214 generates the Alzheimer-specific epitope of antibody AT100 and requires a paired-helical-filament-like conformation. *Eur J Biochem* 252:542–552.
17. Fleming A (1922) On a remarkable bacteriolytic element found in tissues and secretions. *Proc R Soc London Ser B* 93:306–317.
18. Ganz T (2004) Antimicrobial polypeptides. *J Leukoc Biol* 75:34–38.
19. Trexler AJ, Nilsson MR (2007) The formation of amyloid fibrils from proteins in the lysozyme family. *Curr Protein Pept Sci* 8:537–557.
20. Witter MP (2007) The perforant path: Projections from the entorhinal cortex to the dentate gyrus. *Prog Brain Res* 163:43–61.
21. van Groen T, Miettinen P, Kadish I (2003) The entorhinal cortex of the mouse: Organization of the projection to the hippocampal formation. *Hippocampus* 13:133–149.

22. DeToledo-Morrell L, Stoub TR, Wang C (2007) Hippocampal atrophy and disconnection in incipient and mild Alzheimer's disease. *Prog Brain Res* 163:741–753.
23. Braak H, Braak E, Bohl J (1993) Staging of Alzheimer-related cortical destruction. *Eur Neurol* 33:403–408.
24. Braak H, Braak E (1995) Staging of Alzheimer's disease-related neurofibrillary changes. *Neurobiol Aging* 16:271–278, discussion 278–284.
25. Ohm TG (2007) The dentate gyrus in Alzheimer's disease. *Prog Brain Res* 163:723–740.
26. Ginsberg SD, et al. (1999) Accumulation of intracellular amyloid-beta peptide (A beta 1–40) in mucopolysaccharidosis brains. *J Neuropathol Exp Neurol* 58:815–824.
27. Hamano K, Hayashi M, Shioda K, Fukatsu R, Mizutani S (2008) Mechanisms of neurodegeneration in mucopolysaccharidoses II and IIIB: Analysis of human brain tissue. *Acta Neuropathol* 115:547–559.
28. Love S, Bridges LR, Case CP (1995) Neurofibrillary tangles in Niemann-Pick disease type C. *Brain* 118:119–129.
29. Hernandez F, Avila J (2007) Tauopathies. *Cell Mol Life Sci* 64:2219–2233.
30. Paxinos G, Franklin KBJ (2001) *The Mouse Brain In Stereotactic Coordinates* (Academic, San Diego), 2nd Ed.
31. Karsten SL, Kudo LC, Geschwind DH (2008) Gene expression analysis of neural cells and tissues using DNA microarrays. *Curr Protoc Neurosci* Chapter 4:Unit 4.28.
32. Karsten SL, et al. (2003) Global analysis of gene expression in neural progenitors reveals specific cell-cycle, signaling, and metabolic networks. *Dev Biol* 261:165–182.
33. Lobo MK, Karsten SL, Gray M, Geschwind DH, Yang XW (2006) FACS-array profiling of striatal projection neuron subtypes in juvenile and adult mouse brains. *Nat Neurosci* 9:443–452.
34. Sabatti C, Karsten SL, Geschwind DH (2002) Thresholding rules for recovering a sparse signal from microarray experiments. *Math Biosci* 176:17–34.
35. Ganz T, et al. (2003) Increased inflammation in lysozyme M-deficient mice in response to Micrococcus luteus and its peptidoglycan. *Blood* 101:2388–2392.